

# Realization of Bound state In the Continuum induced by vertical symmetry breaking in photonic lattice

R. Mermet-Lyaudoz<sup>1</sup>, F. Dubois<sup>1</sup>, N-V. Hoang<sup>1</sup>, E. Drouard<sup>1</sup>, L. Berguiga<sup>2</sup>, C. Seassal<sup>1</sup>, X. Letartre<sup>1</sup>, P. Viktorovitch<sup>1</sup>, and H. S. Nguyen<sup>1\*</sup>

<sup>1</sup>*Université de Lyon, Institut des Nanotechnologies de Lyon, INL/CNRS, Ecole Centrale de Lyon, 36 avenue Guy de Collongue, 69130 Ecully, France and*

<sup>2</sup>*Université de Lyon, Institut des Nanotechnologies de Lyon, INL/CNRS,*

*INSA-Lyon, 7 avenue Jean Capelle, 69621 Villeurbanne, France*

(Dated: May 13, 2019)

We demonstrate experimentally a new type of Bound state In the Continuum (BIC) which is induced by the vertical symmetry breaking of a photonic crystal slab. Such BIC emerges from the hybridization between Bloch resonances of opposite parities once the vertical symmetry is broken, and is observed in the vicinity of the anticrossing point at the lower hybrid band of the energy-momentum diagram. All experimental results are nicely reproduced by numerical simulations, and in good agreement with an analytical model based on Friedrich-Wintgen framework. Together with the possibility of dispersion engineering by vertical symmetry breaking, our results open the way to tailor photonic states in the entire complex plane to study non-hermitian photonics.

At the dawn of quantum mechanics, von Neumann and Wigner predicted that the solution of Schrödinger equation can support creation of perfect bound states embedded in the continuum spectrum of scattered states [1]. Once considered as a mathematical curiosity, the existence of BICs was explained by Friedrich and Wintgen in 1985 as the result of a destructive interference between two resonances coupled to the same radiation channel [2]. This seminal work has paved the way to study these peculiar localized states in both quantum and classical platforms: atomic and molecular system [3–5], solid-state and mesoscopic physics [6–8], water waves [9] and photonic structures [10–14].

The research on BICs is one of the most active topics of contemporary photonics. Due to its interferential nature, the formation of BICs is strongly related to the symmetries (in-plane and vertical symmetry) of the photonic structure. The early works on BICs in photonic lattice focused mainly on the so-called symmetry-protected BICs which appear at the center of the Brillouin zone (i.e.  $\Gamma$  point) of photonic lattices [15, 16]. The origin of these BICs are very intuitive: they are antisymmetric Bloch resonances of photonic crystal exhibiting an in-plane symmetry, thus cannot couple to plane waves of the radiative continuum. Despite its “trivial” origin, the symmetry-protected BICs have led to the demonstration of fascinating features such as vector-beam lasing emission [17, 18] and exceptional points [19, 20]. Recent research on photonic BICs have turned the focus onto off- $\Gamma$  BIC [10, 16, 21] which can be tuned in the momentum space by modifying the lattice parameters [22, 23]. These works are motivated by both fundamental interest (accidental symmetry [21], topological nature [12]) and device applications (tunable and steerable lasing emission [11, 24, 25]). However, most of reported works on

off- $\Gamma$  BIC only consider the interference between modes of the same vertical parity, thus requires designs having vertical symmetry. Such restriction not only limits the configuration of the photonic stack, but also makes it very challenging for the fabrication and characterization of these structures with suspended slab [11] or matching-index liquid [10].

In 2018, Wang et al reported a theoretical proposal of using TE-TM coupling for conceiving BIC [26]. Although this work considers a complex bilayer design, with only BIC creation at the  $\Gamma$  point, it suggests that in the absence of vertical symmetry, mode coupling will play a crucial role for photonic BIC. Very recently, two different groups have predicted creation of off- $\Gamma$  BICs in the vicinity of anticrossing point arising from the repelling between modes of different diffraction orders [27], or between a photonic mode and a plasmonic mode [14]. At the same time, in the scheme of single sub-wavelength resonator, thus without any lattice, quasi-BIC condition has been discovered and demonstrated experimentally in the microwave domain with the strong mode coupling regime between resonances of different natures [28]. Hinted by these proposals, we expect that off- $\Gamma$  BICs can emerge from the avoided crossing between modes of opposite parities when breaking the vertical symmetry.

In this Letter, we propose a new type of off- $\Gamma$  BIC which does not require a vertical symmetry design. Quite the contrary, this BIC is induced by breaking the vertical mirror symmetry of photonic crystal slab; and is resulted from the coupling between Bloch resonances of opposite vertical parities. In the fabricated sample, the vertical symmetry of the photonic crystal slab is broken due to a partial corrugation along its thickness, combined with the presence of a substrate. The off- $\Gamma$  BIC is experimentally observed in the vicinity of the anticrossing point of the energy-momentum diagram. All of our measurements are nicely reproduced by numerical simulations. Moreover, the experimental results are in perfect agreement with an analytical model based on Friedrich-Wintgen formalism.

\* hai-son.nguyen@ec-lyon.fr

Our results open the way to engineer tunable BICs in photonic structure in the absence of vertical symmetry to study non-hermitian physics.

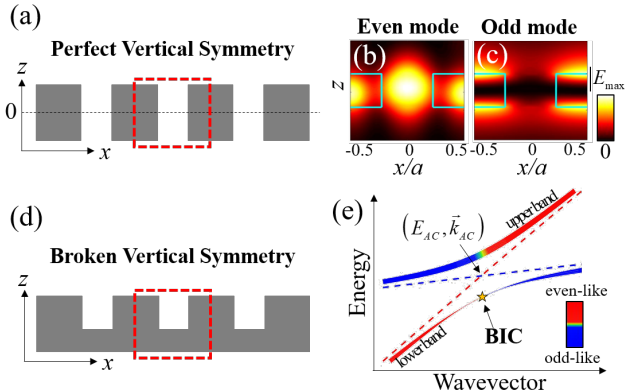


FIG. 1. (a) Sketch of photonic crystal slab with a perfect vertical symmetry breaking. The dashed rectangle corresponds to a unit cell. (b,c) Distribution of the electric field intensity  $|E(x, y = 0, z)|$  of the first (b) even and (c) odd modes of s-polarization in photonic crystal slab of square lattice of air holes. (d) Sketch of photonic crystal slab with broken vertical symmetry. (e) Avoided crossing from the coupling between modes of opposite parities when breaking the vertical symmetry. The color code illustrates the weight of different parities in the corresponding mode. The line thickness represents the radiative losses of the corresponding modes into the radiative continuum. Dashed lines illustrate dispersions of uncoupled modes (red for even mode and blue for odd mode).

We first discuss the principle of off- $\Gamma$  BIC induced by vertical symmetry breaking. In photonic crystal slabs (1D or 2D lattice) presenting vertical symmetry [i.e. mirror symmetry having symmetry plane  $z = 0$  as shown in Fig. 1(a)], Bloch modes are divided into two orthogonal families: even and odd parities. Figures. 1(b,c) depicts two illustrations of the distribution of electric field intensity corresponding to even mode [Fig. 1(b)] and odd mode [Fig. 1(c)]. The vertical symmetry can be broken by simply considering a slab of the same thickness but with partial corrugation along z-axis [Fig. 1(d)]. In the absence of vertical symmetry, the even and odd resonances will be coupled and become hybrid modes. Such coupling results in avoid crossing of the eigenvalues in the complex plane. In the framework of Friedrich-Wintgen, the coupling of odd-like and even-like resonances can be described by a non-hermitian Hamiltonian, given by [16, 29]:

$$H_{FW}(\vec{k}) = \begin{bmatrix} E_e & \kappa \\ \kappa & E_o \end{bmatrix} - i \begin{bmatrix} \gamma_e & \sqrt{\gamma_e \gamma_o} e^{i\psi} \\ \sqrt{\gamma_e \gamma_o} e^{i\psi} & \gamma_o \end{bmatrix} \quad (1)$$

Where  $E_{e(o)}(\vec{k})$ , depending on wavevector  $\vec{k}$ , correspond to the energy-momentum dispersions of the uncoupled even(odd)-like modes;  $\gamma_{e(o)}$  are their radiative losses;  $\kappa$  is the coupling strength, induced by the vertical symmetry breaking; and  $\psi$  is the phase-shift between two modes.

In our system, the two modes are localized in the same slab, thus  $\psi \approx 0$ . This is in contrast to the case of Fabry Perot BIC obtained via coupling between identical but far-apart localized resonances [16, 29–31]. In the following, we assume that  $\psi = 0$ , unless stated otherwise in the discussion part at the end of the paper.

The energy  $E_{upper(lower)}$  and the radiative losses  $\gamma_{upper(lower)}$  are given respectively by the real and imaginary parts of the complex eigenvalues  $\Omega_{upper(lower)}$  of  $H_{FW}$ . From the expression of  $H_{FW}$ , we note that there is a radiative exchange between the two modes and the total radiation rate is conserved:  $\gamma_{upper} + \gamma_{lower} = \gamma_e + \gamma_o$ . The necessary and sufficient conditions for a BIC formation is the Friedrich-Wintgen criterion, given by:

$$E_e - E_o = \frac{\kappa(\gamma_e - \gamma_o)}{\sqrt{\gamma_e \gamma_o}} \quad (2)$$

$$\psi = \pi n \quad (3)$$

where  $n$  is an integer.

In our system, we have assumed that  $\psi = 0$ , thus only eq. (2) to be satisfied. Once such condition is satisfied, the complex eigenvalues of  $H_{FW}$  can be written as:

$$\Omega_{upper} = \frac{E_e + E_o}{2} + \frac{\kappa(\gamma_e + \gamma_o)}{2\sqrt{\gamma_e \gamma_o}} - i(\gamma_e + \gamma_o) \quad (4)$$

$$\Omega_{lower} = \frac{E_e + E_o}{2} - \frac{\kappa(\gamma_e + \gamma_o)}{2\sqrt{\gamma_e \gamma_o}} \quad (5)$$

As consequence, the Friedrich-Wintgen criterion corresponds to an extremist scenario of loss exchange: the upper mode will take all losses (i.e.  $\gamma_{upper} = \gamma_e + \gamma_o$ ) while the lower mode is a BIC (i.e.  $\gamma_{lower} = 0$ ). Moreover, if  $\gamma_e \approx \gamma_o$ , the Friedrich-Wintgen condition of eq. (2) will correspond to  $E_e \approx E_o$ . In this case, with  $\kappa > 0$ , the vertical symmetry breaking will induce a BIC on the lower hybrid mode, in the vicinity of the anticrossing point of midgap energy  $E_{AC}$  and wavevector  $\vec{k} = \vec{k}_{AC}$  [see Fig. 1(e)].

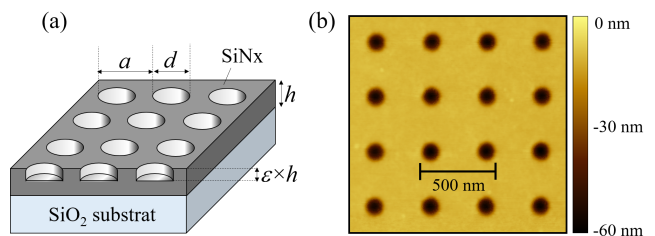


FIG. 2. (a) Sketch of the the fabricated sample, with  $a = 354$  nm,  $d = 160$  nm,  $h = 130$  nm,  $\epsilon = 43\%$ , (b) AFM image of the structure.

To demonstrate experimentally the off- $\Gamma$  BIC induced by vertical symmetry breaking, we employ a similar structure to the one reported for the first observation of off- $\Gamma$  BIC [10]: square lattice of holes in SiNx slab on

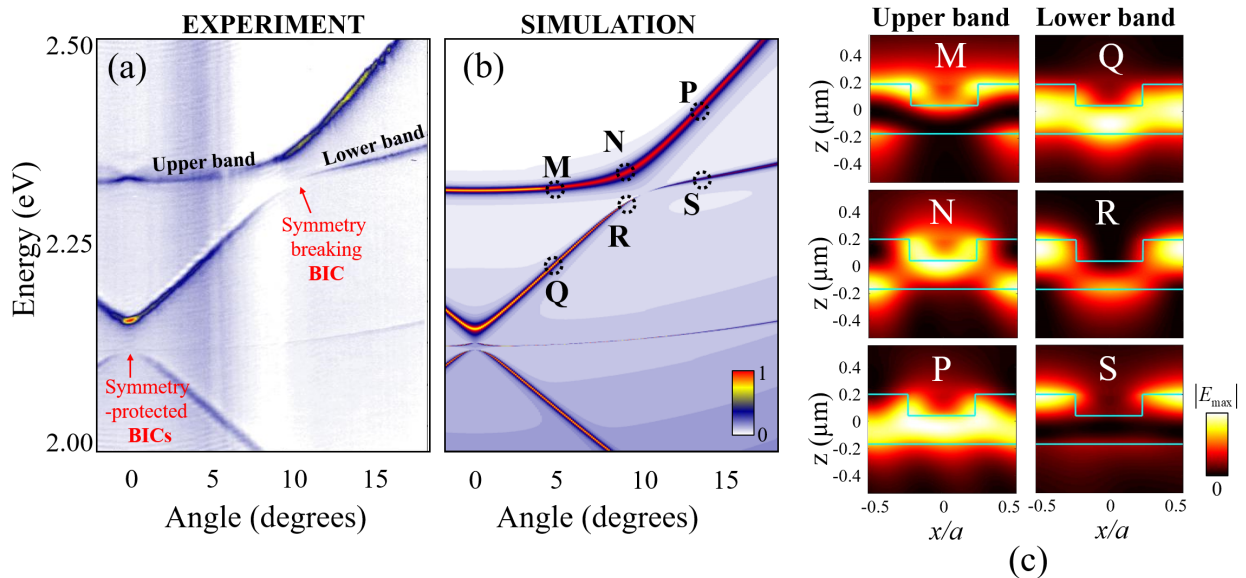


FIG. 3. (a) Experimental measurements and (b) Numerical simulations of the s-polarized angle-resolved reflectivity. (c) Distribution of the electric field intensity  $|E(x, y = 0, z)|$  on different points of the upper and lower band of (b).

glass substrate, but the vertical symmetry of our sample is broken due to a partial etching of the SiNx slab and no use of index matching liquid [see Fig. 2(a)]. Our sample consists of  $h = 130$  nm of SiNx which is deposited on top of fused silica substrate via Plasma-Enhanced Chemical Vapor Deposition. Electron beam lithography and Reactive Ion Etching are used to pattern  $80 \times 80 \mu\text{m}^2$  square lattice of period  $a = 354$  nm and hole diameter  $d = 160$  nm. The etching process is carefully controlled so that the SiNx slab is only partially etched. The etching depth corresponds to a fraction of  $\epsilon = 43\%$  of the total thickness [see Fig. 2(a)].

Angle-resolved reflectivity experiment is performed to obtain the energy-momentum dispersion of the fabricated metasurface. A collimated halogen light is focused onto the photonic crystal structure via a microscope objective (x20, NA=0.42), forming a spot-size of  $20 \mu\text{m}$ . The scattered light is collected via the same objective and its image in Fourier space is projected onto the entrance slit of a spectrometer. The sample orientation is aligned so that the  $\Gamma X$  direction is along the entrance slit. The output of the spectrometer is coupled to a CCD camera, and the image obtained from the camera leads directly to the energy-momentum dispersion diagram along  $\Gamma X$ .

The results of experimental measurement in s-polarization (i.e.  $E_y$ ) are depicted in Fig. 3(a) [32], showing the band dispersion of the first four Bloch resonances. They are Fano resonances resulting from the coupling of Bloch mode with the radiative continuum. Their intensity is proportional to the radiative losses (i.e. coupling strength to the continuum). Three BICs (two at  $\Gamma$  point and one at  $\theta_{BIC} = 9.7^\circ$ ) which correspond to local

vanishings of Fano resonances in the momentum space are observed. The two BICs at  $\Gamma$  point are symmetry-protected BICs and well documented in the literature of square lattice photonic crystals [15]. We now focus our discussion on the off- $\Gamma$  BIC. This BIC is in the vicinity of the anticrossing point between the third and fourth modes. As reported in Ref [15], the third and fourth modes are respectively even (TM-like) and odd (TE-like) modes of square lattice photonic crystal having vertical symmetry. The off- $\Gamma$  BIC is then a symmetry-breaking BIC as described at the beginning of the paper.

To confirm the origin of the observed off- $\Gamma$  BIC, numerical simulations based on Rigorous Coupled Wave Analysis (RCWA) method are performed, using a freely available software package [33]. For these simulations, we use  $n_{SiNx} = 2.03$  and  $n_{SiO2} = 1.46$  as provided by ellipsometry measurements in the considered wavelength range. As shown in Fig. 3(b), the numerical results reproduced perfectly the band diagram of the experimental data and all three BICs mentioned previously are clearly evidenced. Figure 3(c) depicts the distribution of the electric field intensity corresponding to six different points of the upper and lower band [point M, N, P, Q, R and S in Fig. 3(b)]. Comparing these distributions to the ones of even [Fig. 1(b)] and odd [Fig. 1(c)] modes of the design with vertical symmetry, it shows that: i) Far from the anticrossing point, the upper and lower band are either even-like (point Q and P) or odd-like (point M and S); ii) At the anticrossing point (point N and R), the mixing between odd- and even-like parities is balanced. Thus the off- $\Gamma$  BIC observed on the lower band, is indeed resulted from the coupling between modes of opposite parities.

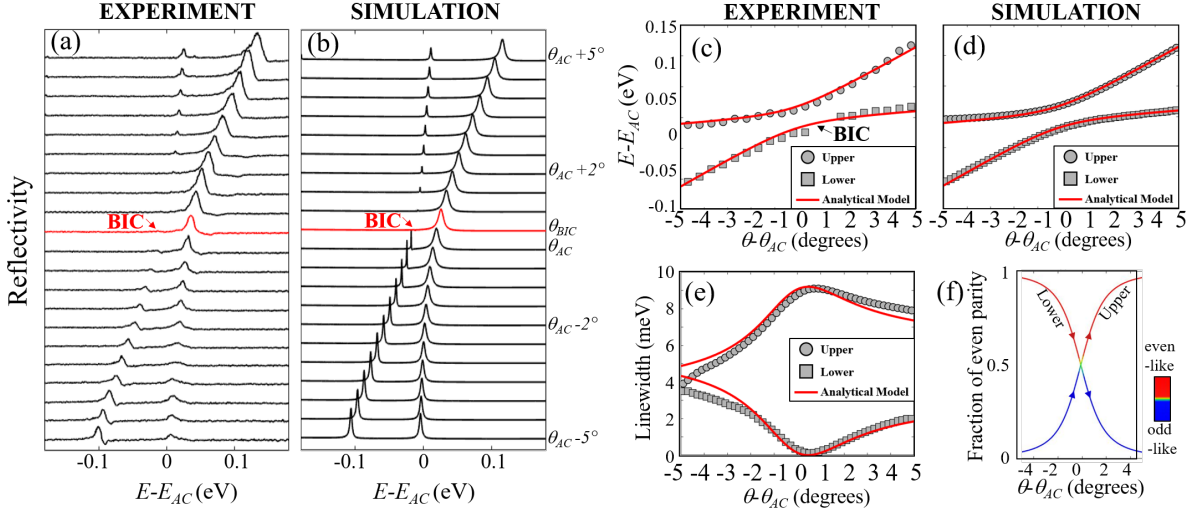


FIG. 4. (a,b) Reflectivity spectra at different incident angles in the vicinity of the anticrossing angle  $\theta_{AC}$ , obtained from (a) experimental measurements, (b) RCWA simulations. (c,d) The energy of the upper and lower band as a function of the incident angle. These data are extracted from resonance peaks in reflectivity spectra of (a,b). The solid red lines correspond to the fittings using the analytic model. (e) The radiative linewidth of the upper and lower band as a function of incident angle. These data are extracted from the resonance peaks in reflectivity spectra of RCWA simulations. The solid red line corresponds to the fitting using the analytic model. All analytic fitting in (c,d,e) has been obtained with a single set of parameters. (f) The fraction of even-like modes in the upper and lower band, calculated using the analytical model.

A deeper insight of the emergence of symmetry-breaking BIC is gained by investigating the experimental and numerical results in the vicinity of the anticrossing point. Figure. 4(a) and (b) represents measured and simulated reflectivity spectra corresponding to incident angles in the range of  $\theta_{AC} \pm 5^\circ$  with a step of  $0.5^\circ$ . Both shows that the BIC is not exactly at the incident angle of the anticrossing but slightly shifted:  $\theta_{BIC} = \theta_{AC} + 0.5^\circ$ . This suggests that the Friedrich-Wintgen criterion of eq. (2) occurs “after” the anticrossing point (i.e.  $E_e > E_o$ ), thus  $\gamma_e$  is slightly larger than  $\gamma_o$ . The complex eigenvalues of the upper and lower band can be extracted from the spectral position and linewidth of resonance peaks of the reflectivity spectra. For the real part, the energy of the upper and lower band as a function of the incident angle are depicted in Fig. 4(c) (for experimental data) and Fig. 4(d) (for numerical data). For the imaginary part, since the experimental resonances exhibit both radiative losses and “non-radiative losses” (i.e. in-plane losses due to the finite size of the excited region and fabrication imperfections), the linewidth of experimental reflectivity peaks overestimates the radiative losses. Thus we only extract the linewidth of the reflectivity peaks from RCWA simulations in which the excited region is considered infinite. These results are obtained by fitting the reflectivity peaks of each angle with Fano profile. Interestingly, as shown in Fig. 4(e), the BIC in the lower band coincides with the maximum of the radiative losses in the upper band. This is in good agreement with loss exchange mechanism at Friedrich-

Wintgen BIC: when one of the hybrid modes becomes lossless, the other takes all the losses.

The validation of the Friedrich-Wintgen nature for our symmetry-breaking BIC is completed with an analytical fitting of the experimental and numerical complex eigenvalues. To minimize the number of fitting parameters, we assume that in the vicinity of the anticrossing point (i.e.  $\theta_{AC} \pm 5^\circ$ ): i) The radiative losses of uncoupled modes  $\gamma_{e(o)}$  varies slowly with the wavevector and can be considered constant; ii) The dispersions of uncoupled modes are linearly changes away from the anticrossing point:  $E_{e(o)}(\theta) = \alpha_{e(o)} \cdot (\theta - \theta_{AC}) + E_{AC}$ . With these hypothesis, the only fitting parameters are  $\kappa$ ,  $\gamma_{e(o)}$  and  $\alpha_{e(o)}$ . The red lines in Fig.3(c,d,e) are the analytical fittings of the real part [Fig.4(c,d)] and imaginary part [Fig.4(e)] with a single set of parameters:  $\kappa = 18$  meV,  $\gamma_e = 5.75$  meV,  $\gamma_o = 3.45$  meV,  $\alpha_e = 1.26$  eV/rad and  $\alpha_o = 0.15$  eV/rad. The theoretical prediction is in good agreement with the experimental and numerical data. The analytical model diverges from the simulation while going away from the anticrossing point in Fig. 4(e). Indeed the linewidths of both even and odd modes are taken constant in our model while it may vary depending on the angle. To illustrate the hybrid nature of the upper and lower band, the fraction of even-like component in each band is calculated from the fitting parameters and represented in Fig. 4(f). This result is coherent with the distribution of electric field intensity in the upper and lower band as discussed previously [Fig. 3(c)]. Moreover, the coupling strength  $\kappa = 18$  meV is also in good agreement with the

value given by numerical estimation [32].

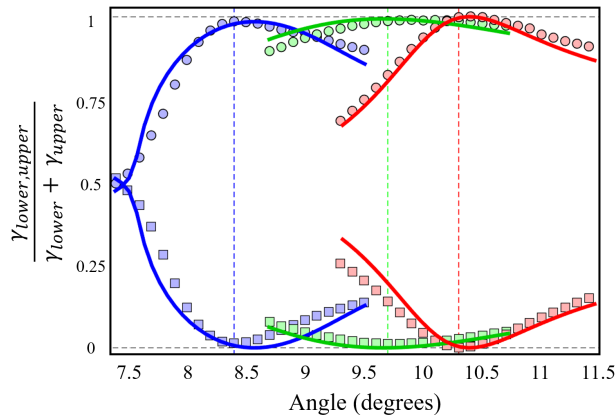


FIG. 5. Evolution of normalized  $\gamma_{lower}$  and  $\gamma_{upper}$  depending on the angle for different aspect-ratios (blue : 0.8; green : 0.5; red = 0.2). Squares and circles stand respectively for the lower and upper modes and full lines are corresponding analytic models. The dotted lines represent the positions of  $\theta_{BIC}$  for the different aspect ratios.

We now discuss on the robustness of the symmetry-breaking BIC. We performed RCWA simulations for the same design [Fig. 2(a)] but with different etching coefficient  $\epsilon$ . For a spectral resolution corresponding to  $Q \sim 10^5$ , the numerical results show that the symmetry-breaking BIC - vanishing of Fano resonance on the dispersion curve - emerges and stays robust for every etching coefficient  $\epsilon$  smaller than  $\epsilon_{max} \approx 65\%$  [32]. But for  $\epsilon > \epsilon_{max}$ , while a minimum/maximum of linewidth of the lower-branch/upper-branch in the vicinity of the anticrossing point is still observed, there is no vanishing of the Fano resonance [32]. As a consequence, the quantum interference always occurs, but we do not have a perfect destructive interference. Indeed, although the two modes are localized in the same slab, the phase-shift  $\psi$  between odd- and even-like modes are extremely small but not exactly zero. An authentic BIC configuration can only be obtained accidentally ( $\psi$  only equal to zero for a given value of  $\epsilon$ ). However, for a broad range of etching factor, the phase-shift is small enough ( $\psi < 0.01\pi$ ), and the diagonalization of the Hamiltonian given by eq. (1) with  $\psi = 0$  is a very good approximation. That explains why the simplified model is enough and reproduces suc-

cessfully the experimental and numerical results. As a matter of fact, except an accidental configuration, the symmetry-breaking BIC is only a quasi-BIC of which the quality factor is very high but not infinite ( $\sim 10^5$  in our sample design). Nevertheless, our results provide an elegant and simple way to obtain quasi-BICs of quality factor high enough for a wide range of photonic applications such as micro-lasers and sensors.

Finally, we investigate the tunability of the reported quasi-BIC. Indeed, by modifying the geometrical parameters (hole diameter  $d$ , total thickness  $h$ ), the effective index of the even and odd-like modes will be changed, leading to a displacement of the anticrossing point in the Fourier space. As a consequence, it is possible to tailor the angular position of the symmetry-breaking BIC for the same stack design. To illustrate such tunability, Fig. 5 represents the angular position  $\theta_{BIC}$  corresponding to different different aspect-ratios  $d/a$  while keeping fix all other parameters. It shows that the BIC can be dragged freely from  $8.4^\circ$  to  $10.3^\circ$ . Again, our simple analytical model reproduces nicely the linewidths obtained from RCWA simulations.

In conclusion, making use of hybridization between Bloch resonances of opposite vertical parities, we have demonstrated experimentally a new type of off- $\Gamma$  Friedrich-Wintgen quasi-BIC that we call symmetry-breaking BIC. This robust and mobile quasi-BIC is simply obtained by working with photonic crystal slab having partial corrugation, and on a substrate. While only consider square lattice design, our concept is directly extended to any type of photonic crystal slab. Moreover, we have recently demonstrated the possibility of tailoring on-demand the real part of photonic dispersion of photonic crystal by the same symmetry breaking action [34]. Combined with the BIC engineering reported in this work, it would open the way to engineer the photonic eigenvalues in the entire complex plan for studying topological features of non-hermitian and parity time symmetry physics [35–37].

The authors would like to thank the staff from the NanoLyon Technical Platform for helping and supporting in all nanofabrication processes, the Consortium Lyon Saint-Etienne de Microscopie (CLYM, FED 4092) for the access to the microscopes and David Albertini for having done the AFM image of the structure. This work is partly supported by the French National Research Agency (ANR) under the projects POPEYE and EMIPERO.

[1] J. Von Neumann and E. Wigner, Z. Phys **30**, 465 (1929).  
[2] H. Friedrich and D. Wintgen, Physical Review A **32**, 3231 (1985).  
[3] H. Friedrich and D. Wintgen, Physical Review A **31**, 3964 (1985).  
[4] L. S. Cederbaum, R. S. Friedman, V. M. Ryaboy, and N. Moiseyev, Physical Review Letters **90**, 013001 (2003).

[5] R. Thomas, M. Chilcott, E. Tiesinga, A. B. Deb, and N. Kjærgaard, Nature Communications **9**, 4895 (2018).  
[6] F. Capasso, C. Sirtori, J. Faist, D. L. Sivco, S.-N. G. Chu, and A. Y. Cho, Nature **358**, 565 (1992).  
[7] J. U. Nöckel, Physical Review B **46**, 15348 (1992).  
[8] M. L. Ladrón de Guevara and P. A. Orellana, Physical Review B **73**, 205303 (2006).

- [9] P. J. COBELLI, V. PAGNEUX, A. MAUREL, and P. PETITJEANS, *Journal of Fluid Mechanics* **666**, 445 (2011).
- [10] C. W. Hsu, B. Zhen, J. Lee, S.-l. Chua, S. G. Johnson, J. D. Joannopoulos, and M. Soljačić, *Nature* **499**, 188 (2013).
- [11] A. Kodigala, T. Lepetit, Q. Gu, B. Bahari, Y. Fainman, and B. Kanté, *Nature* **541**, 196 (2017).
- [12] B. Zhen, C. W. Hsu, L. Lu, a. D. Stone, and M. Soljačić, *Physical Review Letters* **113**, 1 (2014).
- [13] J. Gomis-Bresco, D. Artigas, and L. Torner, *Nature Photonics* **11**, 232 (2017).
- [14] S. I. Azzam, V. M. Shalaev, A. Boltasseva, and A. V. Kildishev, *Physical Review Letters* **121**, 253901 (2018), arXiv:1808.08244.
- [15] J. Lee, B. Zhen, S. L. Chua, W. Qiu, J. D. Joannopoulos, M. Soljačić, and O. Shapira, *Physical Review Letters* **109**, 1 (2012).
- [16] C. W. Hsu, B. Zhen, A. D. Stone, J. D. Joannopoulos, and M. Soljačić, *Nature Reviews Materials* **1**, 16048 (2016).
- [17] T.-P. Vo, A. Rahmani, A. Belarouci, C. Seassal, D. Nedeljkovic, and S. Callard, *Optics Express* **18**, 26879 (2010).
- [18] S. Iwahashi, Y. Kurosaka, K. Sakai, K. Kitamura, N. Takayama, and S. Noda, *Optics Express* **19**, 11963 (2011).
- [19] B. Zhen, C. W. Hsu, Y. Igarashi, L. Lu, I. Kaminer, A. Pick, S.-L. Chua, J. D. Joannopoulos, and M. Soljačić, *Nature* **525**, 354 (2015).
- [20] H. Zhou, C. Peng, Y. Yoon, C. W. Hsu, K. A. Nelson, L. Fu, J. D. Joannopoulos, M. Soljačić, and B. Zhen, *Science* **359**, 1009 (2018).
- [21] Y. Yang, C. Peng, Y. Liang, Z. Li, and S. Noda, *Physical Review Letters* **113**, 037401 (2014).
- [22] C. Blanchard, J.-P. Hugonin, and C. Sauvan, *Physical Review B* **94**, 155303 (2016).
- [23] L. Ni, Z. Wang, C. Peng, and Z. Li, *Physical Review B* **94**, 1 (2016).
- [24] B. Bahari, F. Vallini, T. Lepetit, R. Tellez-Limon, J. H. Park, A. Kodigala, Y. Fainman, and B. Kante, (2017), arXiv:1707.00181.
- [25] S. T. Ha, Y. H. Fu, N. K. Emani, Z. Pan, R. M. Bakker, R. Paniagua-Domínguez, and A. I. Kuznetsov, *Nature Nanotechnology* (2018), 10.1038/s41565-018-0245-5.
- [26] H. F. Wang, S. K. Gupta, X. Y. Zhu, M. H. Lu, X. P. Liu, and Y. F. Chen, *Physical Review B* **98**, 1 (2018).
- [27] E. N. Bulgakov and D. N. Maksimov, *Physical Review A* **98** (2018), 10.1103/PhysRevA.98.053840, arXiv:1808.03180.
- [28] A. A. Bogdanov, K. L. Koshelev, P. V. Kapitanova, M. V. Rybin, S. A. Gladyshev, Z. F. Sadrieva, K. B. Samusev, Y. S. Kivshar, and M. F. Limonov, *Advanced Photonics* **1**, 1 (2019).
- [29] K. Koshelev, G. Favraud, A. Bogdanov, Y. Kivshar, and A. Fratallocchi, *Nanophotonics* (2019), 10.1515/nanoph-2019-0024.
- [30] Y. Shuai, D. Zhao, A. Singh Chadha, J. H. Seo, H. Yang, S. Fan, Z. Ma, and W. Zhou, *Applied Physics Letters* **103**, 24582 (2013).
- [31] L. S. Li and H. Yin, *Scientific Reports* **6**, 1 (2016).
- [32] See Supplemental Materials at (link) for further details on experimental results with p-polarized reflectivity, robustness of symmetry-breaking BIC at different etching coefficient and a numerical estimation of the coupling strength  $\kappa$ .
- [33] V. Liu and S. Fan, *Computer Physics Communications* **183**, 2233 (2012).
- [34] H. S. Nguyen, F. Dubois, T. Deschamps, S. Cuff, A. Pardon, J. L. Leclercq, C. Seassal, X. Letartre, and P. Viktorovitch, *Physical Review Letters* **120**, 66102 (2018), arXiv:1711.07588.
- [35] H. Shen, B. Zhen, and L. Fu, *Physical Review Letters* **120**, 146402 (2018), arXiv:1706.07435.
- [36] L. Feng, R. El-Ganainy, and L. Ge, *Nature Photonics* **11**, 752 (2017).
- [37] B. Midya, H. Zhao, and L. Feng, *Nature Communications* **9**, 8 (2018), arXiv:1011.1669.